

Towards MRI temperature mapping in real time—the proton resonance frequency method with undersampled radial MRI and nonlinear inverse reconstruction

Zhongshuai Zhang¹, Thomas Michaelis¹, Jens Frahm^{1,2}

¹Biomedizinische NMR Forschungs GmbH am Max-Planck-Institut für biophysikalische Chemie, Göttingen, Germany; ²DZHK (German Center for Cardiovascular Research), partner site Göttingen, Göttingen, Germany

Correspondence to: Jens Frahm. Biomedizinische NMR Forschungs GmbH am Max-Planck-Institut für biophysikalische Chemie, Göttingen 37070, Germany. Email: jfracm@gwdg.de.

Background: Optimal control of minimally invasive interventions by hyperthermia requires dynamic temperature mapping at high temporal resolution.

Methods: Based on the temperature-dependent shift of the proton resonance frequency (PRF), this work developed a method for real-time MRI thermometry which relies on highly undersampled radial FLASH MRI sequences with iterative image reconstruction by regularized nonlinear inversion (NLINV). As a first step, the method was validated with use of a temperature phantom and *ex vivo* organs (swine kidney) subjected to heating by warm water or a pulsed laser source.

Results: The temperature maps obtained by real-time PRF MRI demonstrate good accuracy as independently controlled by fiber-optic temperature sensors. Moreover, the dynamic results demonstrate both excellent sensitivity to single laser pulses (20 ms duration, 6 J energy output) and high temporal resolution, i.e., 200 ms acquisition times per temperature map corresponding to a rate of 5 frames per second. In addition, future extensions to *in vivo* applications were prepared by addressing the breathing-related motion problem by a pre-recorded library of reference images representative of all respiratory states.

Conclusions: The proposed method for real-time MRI thermometry now warrants further developments towards *in vivo* MRI monitoring of thermal interventions in animals.

Keywords: Hyperthermia; temperature mapping; thermometry; radial MRI; real-time MRI

Submitted Feb 25, 2017. Accepted for publication Mar 09, 2017.

doi: 10.21037/qims.2017.03.03

View this article at: <http://dx.doi.org/10.21037/qims.2017.03.03>

Introduction

Recent developments in MRI provide a new method for real-time imaging (1) which offers so far unsurpassed diagnostic capabilities in a large variety of clinical fields. Respective applications range from cardiac MRI without ECG synchronization and during free breathing (2) to real-time studies of blood flow (3), swallowing (4), dysphagia (5), esophageal functions (6), dynamics of the temporomandibular joint (7), respiration-induced flow of the cerebrospinal fluid (8,9) as well as movements of the articulators during normal speech (10) or brass playing

of patients with embouchure dystonia (11). In a technical sense, the method is based on highly undersampled radial gradient-echo sequences in combination with iterative image reconstruction by nonlinear inversion (NLINV) and temporal regularization (1). These new possibilities are expected to vastly broaden the range of clinical MRI and, in particular, to stimulate renewed interest in “interventional MRI”, i.e., the use of real-time MRI for monitoring and guiding minimally invasive procedures.

In this sense, true “real-time” MRI not only refers to high-speed data acquisitions, but includes (I) online

reconstruction and display of images on existing MRI systems; (II) with negligible delay; (III) at user-selectable spatiotemporal resolutions and contrasts; and (IV) without expert knowledge. Obviously, real-time MRI of anatomic details in freely selectable image orientations should directly be applicable to diagnostic procedures such as an MRI-guided biopsy. In order to move the approach even further towards therapeutic interventions, additional prerequisites have to be solved. Most importantly, this refers to real-time MRI mapping of tissue temperature in response to thermal techniques involving the exposure to radiofrequency (12), high intensity focused ultrasound (13) or laser light (14,15). In this context, the present work focuses on temperature changes during hyperthermia which result in coagulation rather than vaporization or ablation of the target tissue.

The aim of this first study was to develop the key elements for real-time MRI temperature mapping based on the temperature-dependent shift of the proton resonance frequency (PRF) (16). This choice is in full agreement with the technical and clinical considerations outlined in a recent review (17). The PRF method is an alternative to T1-dependent temperature changes (18-20). This latter method was also studied (21) but discarded for real-time applications as its temporal resolution is limited to several seconds by the need to acquire and reconstruct a full inversion-recovery or saturation-recovery MRI experiment. In contrast, this study achieved temperature difference maps every 200 ms corresponding to a rate of 5 frames per second. The results are validated on phantoms and *ex vivo* organs, while future *in vivo* extensions are prepared by a novel approach to deal with motion-induced phase errors.

Material and methods

MRI

All measurements were performed on a 3 T MRI system (Magnetom Prisma Fit, Siemens Healthcare, Erlangen, Germany) using either a 64-channel head coil or a combination of an 18-element thorax coil with suitable coils of the 32-element spine array.

Undersampled radial FLASH MRI sequences (1) with dual-echo acquisitions were applied to simultaneously acquire an anatomic and a temperature-sensitive image. Online image reconstruction by NLINV took advantage of a bypass computer (sysGen/TYAN Octuple-GPU, Sysgen, Bremen, Germany) equipped with eight graphical

processing units (GeForce GTX, TITAN Black, NVIDIA, Santa Clara, CA). This bypass computer has been fully integrated into the reconstruction pipeline of the commercial MRI system by a single network connection. It is automatically used when selecting a real-time MRI sequence with NLINV reconstruction and therefore operates without any expert knowledge or user interference. The current NLINV reconstruction speed is up to 55 frames per second depending on image matrix. Online image display is accomplished with a minimal delay of about 2 frames on arbitrary monitors (e.g., inside the scanner room).

At this stage, i.e., for the present results, the actual temperature maps were still obtained offline by taking phase differences to a reference phase map. For experimental validations with use of a water phantom and *ex vivo* organs, reference MRI data was obtained before heating. For post-processing, a temporal median filter was applied on both the temperature maps and magnitude images.

Image reconstruction

For a dual-echo acquisition, the MRI signal can be expressed as

$$S_{i,j}(t) = \int \rho_i(\vec{r}) \cdot C_j(\vec{r}) \cdot e^{-i2\pi k(t)\vec{r}} d\vec{r} \quad [1]$$

with $i \in [1, 2], j \in [1, N]$

where $S_{i,j}$ is the acquired raw data of the i^{th} echo and the j^{th} coil, while $\rho_i(\vec{r})$ represents the image content of the i^{th} echo, $C_j(\vec{r})$ represents the coil sensitivity of the j^{th} coil and $k(t)$ is the sampled k -space data. Similar to (1), with ρ_i and C_j as unknowns, Eq. [1] can be simplified as

$$F(x) = y \text{ with } x = \begin{pmatrix} \rho_1 \\ \rho_2 \\ C_1 \\ \vdots \\ C_N \end{pmatrix} \quad [2]$$

with x the unknowns, y the sampled k -space data and F the forward operator which converts the estimated unknowns to the corresponding k -space data. To solve this nonlinear inverse problem, we applied the Gauss-Newton method which linearizes Eq. [2] and leads to the corresponding cost function

$$\Phi(dx) = \left\| DF(x_n) dx - (y - F(x_n)) \right\|_2^2 \quad [3]$$

Here, x_n is the estimate from the n^{th} Newton step and $DF(x_n)$ is the Fréchet derivative of F at x_n . Tikhonov regularization is then employed to the cost function, which is rewritten as

$$\Phi(dx) = \left\| DF(x_n) dx - (y - F(x_n)) \right\|_2^2 + \|x_n + dx - x_0\|_2^2 \quad [4]$$

The initial guess x_0 is the estimate from the previous frame weighted by a damping factor $0 \leq p \leq 1$. Eq. [4] is solved by the conjugate gradient method. In the present work, and in agreement with real-time phase-contrast flow MRI studies (3), seven Newton steps and a damping factor of 0.7 were used for image reconstruction. In order to reduce the computation time of the NLINV reconstruction without compromising image quality, ten virtual coils (channels) were defined by a principal component analysis method (1).

Calculation of temperature maps

In a first step the complex image of a certain coil (M_j) is calculated by multiplying the image content (ρ_2) with the corresponding coil sensitivity (C_j). The phase difference ($\Delta\phi$) between the current temperature and the reference data is then calculated according to

$$\Delta\phi = \arg \left[\sum_{j=0}^N (M_{i,j} \cdot M_{0,j}^*) \right] \quad [5]$$

with $M_{1,j}$ and $M_{0,j}$ the complex image of the j^{th} coil for the current temperature and the reference data, respectively, and * the complex conjugate. Subsequently, the temperature change (ΔT) can be calculated according to (16)

$$\Delta T = \frac{\Delta\phi}{\alpha\gamma B_0 TE} \quad [6]$$

with a temperature coefficient $\alpha = -0.01$ ppm/ $^{\circ}\text{C}$, γ the gyromagnetic ratio, B_0 the magnetic field and TE the echo time.

Phantom studies

A homemade cylindrical phantom (14 cm diameter) was used for quantitatively evaluating the PRF-derived temperature differences along a spatial temperature gradient generated by a central tube with warm flowing water (50 $^{\circ}\text{C}$). To avoid complications from turbulent flow, the inner cylinder (diameter 7 cm) was filled with 2% agarose (doped with 0.5 mM/L CuSO_4). Three fiber optic sensors (OPT-M,

OPSENS, Quebec, Canada) were aligned in radial positions at 1, 2 and 3 cm distance to the central tube and used to measure local temperature changes. The outer cylinder was cooled by flowing water at room temperature. Stable temperature conditions were achieved after about two hours. Four outer reference tubes with the same agarose filling served to compensate for any field drift during prolonged measurements (22).

The phantom was located in the head coil of the MRI scanner with its longitudinal axis parallel to the main magnetic field. As shown in *Figure 1*, MRI temperature mapping was performed in a transverse plane, perpendicular to the central tube and surrounding cylinders, using the following parameters: TE/TR = 10.0/11.8 ms, flip angle 10 $^{\circ}$, FOV 192 \times 192 mm 2 , slice thickness 6 mm, in-plane resolution 1.5 \times 1.5 mm 2 , number of radial spokes 17, acquisition time 200 ms per temperature difference map.

Ex vivo studies

Fresh swine kidneys were used for *ex vivo* experiments. In a first setting a plastic tube (inner diameter 4 mm, wall thickness 1 mm) providing warm water (60 $^{\circ}\text{C}$) was inserted into the kidney along its long axis. In order to independently record the temperature of the kidney, a fiber optic sensor was positioned parallel to the water tube at a distance of about 5 mm. The following MRI parameters were used: TE/TR = 10.0/11.8 ms, flip angle 10 $^{\circ}$, FOV 128 \times 128 mm 2 , slice thickness 6 mm, in plane resolution 1 \times 1 mm 2 , number of radial spokes 17, acquisition time 200 ms per temperature map. Once the pump was turned on, MRI acquisitions were started every 3 min until 30 min.

In a second series of *ex vivo* experiments, a commercial semiconductor laser (RevoLix jr.30, LISA laser products OHG, Katlenburg-Lindau, Germany) with a wavelength of 2 μm was used to achieve focal heating (23,24). The laser was located outside the MRI scanner room and the thermal energy was transmitted by a thin and flexible laser fiber (outer diameter 0.75 mm) of 10 m length. For focal heating of the kidney cortex the fiber penetrated about 10 mm into the kidney. The laser was first operated in a continuous pulsed mode with the following parameters: output power 2 W, repetition rate 20 Hz, pulse duration 20 ms, pulsing time 180 s and total energy 144 J. Studies using a single-pulse mode employed the following parameters: output power 30 W, pulse duration 200 ms and output energy 6 J per pulse. Dual-echo MRI was performed with the following parameters: TE $_1$ /TE $_2$ /TR = 2.64/10.0/11.9 ms,

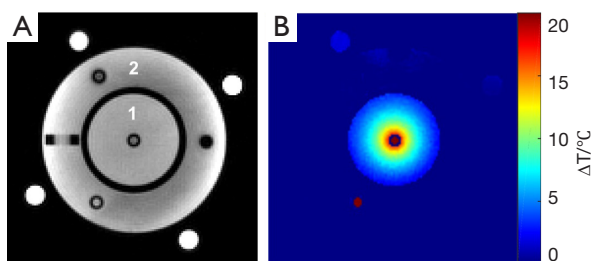


Figure 1 Temperature phantom. (A) Magnitude image of the temperature phantom after 2 h of heating; (B) the corresponding temperature difference map (PRF method) reveals the expected cylindrically symmetric temperature gradient within the agarose-filled inner cylinder [1] between the hot water-filled tube in the center and the cold water in the outer compartment [2]. The high temperature in the lower left tube in the outer cold water (red spot) is due to the out-flowing warm water.

flip angle 10° , FOV $128 \times 128 \text{ mm}^2$, slice thickness 3 mm, in plane resolution $0.5 \times 0.5 \text{ mm}^2$, number of radial spokes 17, acquisition time 200 ms per temperature map.

Human motion

A volunteer without known illness was recruited from the local University. Informed written consent was obtained prior to all experiments according to the regulations of the local ethical committee. Serial images of the abdomen during free breathing were obtained in a coronal plane for a period of 100 s to demonstrate prominent respiratory movements. The MRI parameters for temperature mapping (without heating) were: $TE_1/TE_2/TR = 2.64/10.0/11.9 \text{ ms}$, flip angle 10° , FOV $256 \times 256 \text{ mm}^2$, slice thickness 5 mm, in-plane resolution $0.5 \times 0.5 \text{ mm}^2$, number of radial spokes 17, acquisition time 200 ms per temperature map. The magnitude images of the first echo, which were acquired during the first 90 s, served as a library of reference images representing different states of respiration. Subsequent acquisitions (10 s) were used to obtain temperature difference maps by selecting a reference image from the library which is closest to the respiratory state of the actual image. This was accomplished by calculating cross-correlation coefficients between the first gradient-echo image of the actual scan and all images in the library (25). After identification of the best match the phase of the corresponding second (temperature-sensitive) gradient-echo image was used for temperature calculation.

Results

Figure 1 shows a temperature difference map of the experimental temperature phantom which was obtained after two hours of cycling cold and warm water. Fiber-optic temperature sensors at 1, 2, and 3 cm distance from the central tube of warm water revealed temperature increases of 12.2, 7.1, and 3.8 $^\circ\text{C}$, respectively, which were in excellent agreement with the results obtained by the PRF method, i.e., 11.6 ± 0.9 , 7.1 ± 0.5 , and $3.9 \pm 0.3 \text{ }^\circ\text{C}$. As implemented here, the PRF method allows for monitoring temperature changes of about $\pm 39 \text{ }^\circ\text{C}$ relative to room (or body) temperature without phase wrapping. This is in accordance with the range required for hyperthermia-based therapies (26).

As demonstrated in Figure 2, the PRF method was also validated for heating an *ex vivo* swine kidney by cycling 30 min of warm water ($60 \text{ }^\circ\text{C}$) through an inserted tube. Again, the relative temperature increases obtained by real-time MRI temperature mapping and the fiber-optic sensors were in close agreement as shown in the bottom part of Figure 2.

The effects of focal heating in a region of the kidney cortex are shown in Figure 3. The increase of tissue temperature during continuous pulsing of laser light for a period of 180 s was clearly resolved and restricted to a small region near the tip of the fiber. Within the first 40 s the temperature increased rapidly by about $14 \text{ }^\circ\text{C}$ and further to $17 \text{ }^\circ\text{C}$ after 90 s. Despite continuous laser pulsing, the thermal equilibrium established at about $20 \text{ }^\circ\text{C}$ after 120 s of pulsing remained stable until the end of the experiment, when the temperature decreased towards room temperature.

In order to take full advantage of the 200 ms resolution achievable by real-time MRI, relative temperature changes were also investigated in response to single laser pulses. As demonstrated in Figure 4, the PRF method detected a focal temperature increase of about $5 \text{ }^\circ\text{C}$ to a 200 ms laser pulse of 6 J energy within a period of about 1 to 2 s. When repeated every 20 s, the applied energy resulted in a cumulative temperature rise to about $12 \text{ }^\circ\text{C}$ after three pulses. This behavior and its visualization by real-time MRI open the possibility to adjust the temperature in the target tissue not only by varying the laser power, but also by changing the inter-pulse delay. In particular, this will allow for timely interactions to unexpected temperature changes during surgical treatment.

Attempts to obtain temperature difference maps of the human abdomen *in vivo* suffered from phase differences due

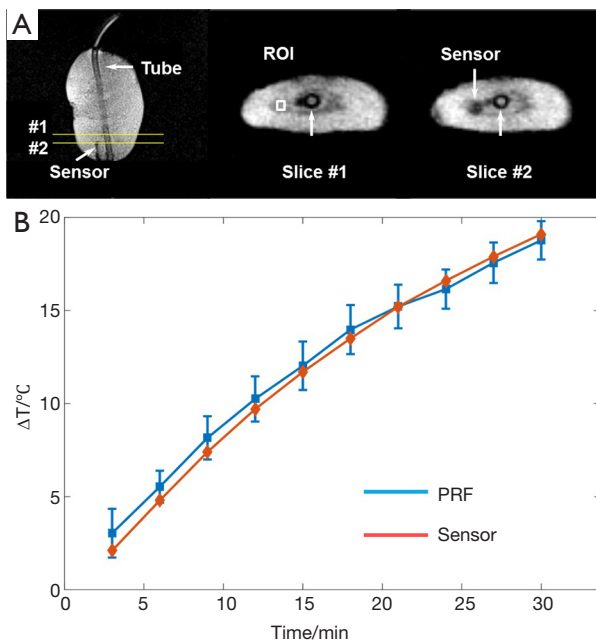


Figure 2 *Ex vivo* swine kidney. (A) Coronal and transverse images of an *ex vivo* kidney showing the position of the warm water tube, the region of interest for analysis (slice #1) and the temperature sensor (slice #2); (B) the relative temperature differences during 30 min of heating were almost identical for the PRF method (blue) and the fiber-optic temperature sensor (red).

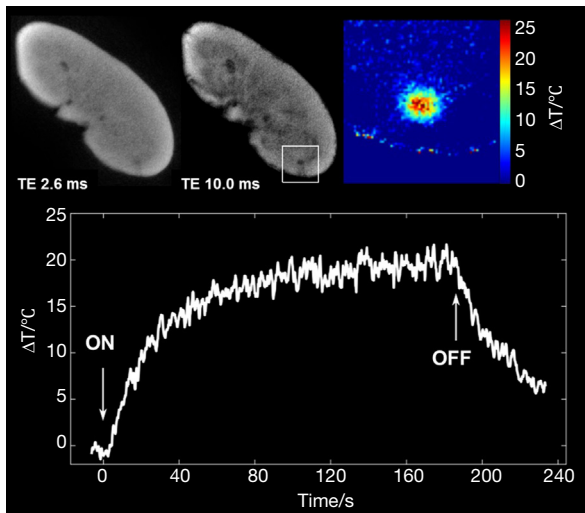


Figure 3 Continuous laser heating. (Top) Coronal magnitude images (echo times TE) of an *ex vivo* swine kidney and corresponding magnified temperature difference map after continuous focal laser heating (180 s, 144 J). (Bottom) The PRF-based time course of laser-induced temperature changes next to the tip of the laser fiber shows a steep increase within the first 40 s and a plateau at about 20 °C after 120 s.

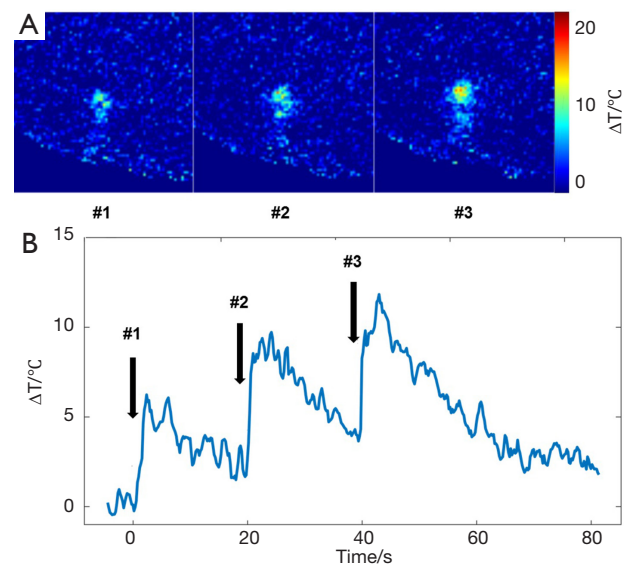


Figure 4 Pulsed laser heating. (A) Magnified temperature difference maps of an *ex vivo* swine kidney after applying three focal laser pulses #1, #2 and #3 (200 ms, 6 J each) every 20 s; (B) the PRF-based time course of laser-induced temperatures changes next to the tip of the laser fiber shows a rapid increase within the first 1 to 2 s followed by a slower decrease. Together, the laser pulses resulted in a cumulative temperature rise of about 12 °C.

to breathing movements, which are mistaken as temperature changes. This problem is clearly demonstrated by the two images and the resulting temperature difference map shown in the top row of *Figure 5*. It may be circumvented by using a pre-recorded set of images which is representative of all respiratory states during breathing. For the actual temperature study, the baseline image with the highest correlation coefficient to the current scan (early gradient-echo image) is then taken as reference for calculating a phase difference map using the corresponding temperature-sensitive late gradient-echo images. As shown in the bottom part of *Figure 5*, this approach dramatically reduces any movement-induced phase differences and provides much more reliable temperature difference maps, i.e., zero temperature changes in a situation without heating.

Discussion

The present work offers basic solutions for MRI thermometry at high temporal resolution. Based on the PRF method, real-time MRI thermometry was established at 200 ms resolution with high sensitivity to temperature

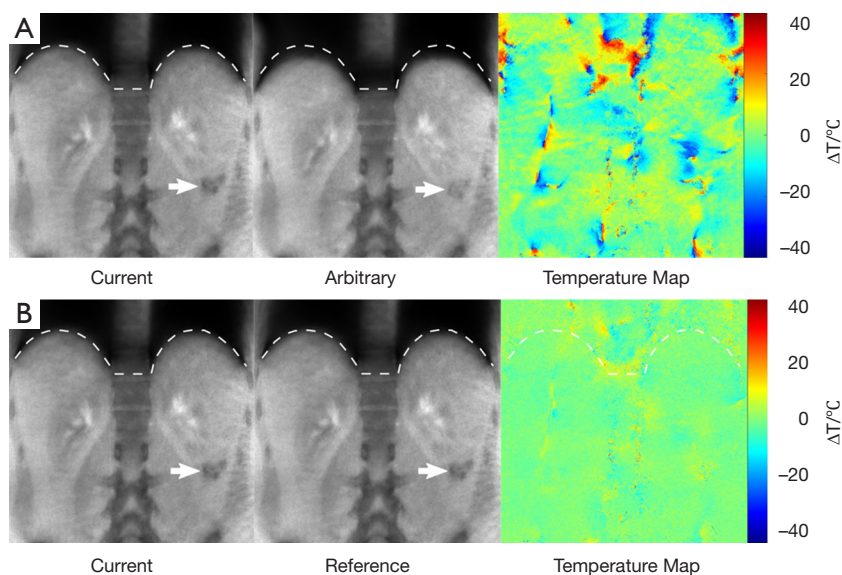


Figure 5 *In vivo* motion artifacts. (A) A coronal magnitude image and an arbitrary reference image of a human abdomen selected for calculating a PRF-based temperature difference map. Without heating the map should be zero, but presents with motion-induced phase errors due to breathing; (B) the same magnitude image as above, a reference image selected by cross-correlation from a library of pre-recorded images at different respiratory states, and the resulting temperature difference map with much reduced phase errors.

increases elicited by a single laser pulse of 6 J energy output. As the established online reconstruction of images will soon be complemented by an online calculation of temperature difference maps, the approach promises immediate feedback about the achieved tissue temperature which will allow for a quick detection of remote hot spots or interactive correction of undesired effects such as overheating. Alternatively, the high temporal resolution may be exploited to interleave MRI temperature mapping with other measurements such as, for example, anatomic real-time MRI at different tissue contrasts or 3D localizations of surgical devices by spatially encoded phase-contrast MRI (27).

A most useful extension of the PRF method described here should deal with improved volume coverage. Again at the expense of some temporal resolution, the acquisition scheme may be developed towards multi-slice real-time MRI thermometry using, for example, three parallel or even orthogonal sections. Such strategies not only cover out-of-plane movements, but also depict neighboring blood vessels or fat and further account for undesired heat transport to adjacent tissue in directions perpendicular to the image orientation. Of course, also other clinically desirable options as, for example, fat suppression may easily be incorporated into the real-time PRF method as such modules require less than 15 ms per image acquisition.

At this stage, a transient technical limitation has been the offline calculation of the temperature difference maps. However, as similar problems have already been solved for the online calculation of velocity maps using real-time phase-contrast flow MRI (3), rapid progress with use of our integrated GPU bypass computer is foreseeable. In fact, parallelization of the algorithm will even allow for a model-based reconstruction technique (21) which is expected to further improve the PRF method in terms of SNR and spatiotemporal acuity as previously demonstrated for phase-contrast flow MRI (28). Because model-based reconstructions exploit redundancy in the data, they promise multi-slice temperature mapping without a major trade-off in temporal resolution or image quality.

Most importantly, the current developments now warrant further steps towards MRI monitoring of thermal interventions in humans. The next obvious level should involve *in vivo* animal studies to deal with tissue cooling or heat transport by blood flow and phase disturbances by movements of the interventional instrument, target tissue or overall body. While this work describes a promising though preliminary method to overcome the effects of respiratory motion, it remains to be seen which additional strategies will be necessary to reliably map temperature differences under clinical conditions. This particularly holds true for

more accurate assessments of target movements in three dimensions (29).

Acknowledgements

We are grateful to Heinrich-Otto Teichmann (LISA laser products OHG) for providing the laser system and thank Klaus-Dietmar Merboldt and Roland Tammer for helpful discussions about the temperature phantom.

Footnote

Conflicts of Interest: J Frahm is a co-inventor of the real-time MRI patent used here. The other authors have no conflicts of interest to declare.

References

1. Uecker M, Zhang S, Voit D, Karaus A, Merboldt KD, Frahm J. Real-time MRI at a resolution of 20 ms. *NMR Biomed* 2010;23:986-94.
2. Zhang S, Joseph AA, Voit D, Schaez S, Merboldt KD, Unterberg-Buchwald C, Hennemuth A, Lotz J, Frahm J. Real-time magnetic resonance imaging of cardiac function and flow-recent progress. *Quant Imaging Med Surg* 2014;4:313-29.
3. Untenberger M, Tan Z, Voit D, Joseph AA, Roeloffs V, Merboldt KD, Schätz S, Frahm J. Advances in real-time phase-contrast flow MRI using asymmetric radial gradient echoes. *Magn Reson Med* 2016;75:1901-8.
4. Olthoff A, Zhang S, Schweizer R, Frahm J. On the physiology of normal swallowing as revealed by magnetic resonance imaging in real time. *Gastroenterol Res Pract* 2014;2014:493174.
5. Olthoff A, Carstens PO, Zhang S, von Fintel E, Friede T, Lotz J, Frahm J, Schmidt J. Evaluation of dysphagia by novel real-time MRI. *Neurology* 2016;87:2132-8.
6. Zhang S, Joseph AA, Gross L, Ghadimi M, Frahm J, Beham AW. Diagnosis of gastroesophageal reflux disease using real-time magnetic resonance imaging. *Sci Rep* 2015;5:12112.
7. Krohn S, Gersdorff N, Wassmann T, Merboldt KD, Joseph AA, Buegers R, Frahm J. Real-time MRI of the temporomandibular joint at 15 frames per second-A feasibility study. *Eur J Radiol* 2016;85:2225-30.
8. Niebergall A, Zhang S, Kunay E, Keydana G, Job M, Uecker M, Frahm J. Real-time MRI of speaking at a resolution of 33 ms: undersampled radial FLASH with nonlinear inverse reconstruction. *Magn Reson Med* 2013;69:477-85.
9. Iltis PW, Frahm J, Voit D, Joseph A, Schoonderwaldt E, Altenmüller E. Divergent oral cavity motor strategies between healthy elite and dystonic horn players. *J Clin Mov Disord* 2015;2:15.
10. Dreha-Kulaczewski S, Joseph AA, Merboldt KD, Ludwig HC, Gärtner J, Frahm J. Inspiration is the major regulator of human CSF flow. *J Neurosci* 2015;35:2485-91.
11. Dreha-Kulaczewski S, Joseph AA, Merboldt KD, Ludwig HC, Gärtner J, Frahm J. Identification of upward movement of human cerebrospinal fluid in vivo and its relation to the brain venous system. *J Neurosci* 2017;37:2395-402.
12. Vigen KK, Jarrard J, Rieke V, Frisoli J, Daniel BL, Butts Pauly K. In vivo porcine liver radiofrequency ablation with simultaneous MR temperature imaging. *J Magn Reson Imaging* 2006;23:578-84.
13. Dragonu I, de Oliveira PL, Laurent C, Mougenot C, Grenier N, Moonen CT, Quesson B. Non-invasive determination of tissue thermal parameters from high intensity focused ultrasound treatment monitored by volumetric MRI thermometry. *NMR Biomed* 2009;22:843-51.
14. Peters RD, Chan E, Trachtenberg J, Jothy S, Kapusta L, Kucharczyk W, Henkelman RM. Magnetic resonance thermometry for predicting thermal damage: an application of interstitial laser coagulation in an in vivo canine prostate model. *Magn Reson Med* 2000;44:873-83.
15. Jakob PM, Hendrich C, Breiting T, Schäfer A, Berden A, Haase A. Real time monitoring of laser-induced thermal changes in cartilage in vitro by using snapshot FLASH. *Magn Reson Med* 1997;37:805-8.
16. Ishihara Y, Calderon A, Watanabe H, Okamoto K, Suzuki Y, Kuroda K, Suzuki Y. A precise and fast temperature mapping using water proton chemical shift. *Magn Reson Med* 1995;34:814-23.
17. Yuan J, Mei CS, Panych LP, McDannold NJ, Madore B. Towards fast and accurate temperature mapping with proton resonance frequency-based MR thermometry. *Quant Imaging Med Surg* 2012;2:21-32.
18. Cline HE, Hynynen K, Hardy CJ, Watkins RD, Schenck JF, Jolesz FA. MR temperature mapping of focused ultrasound surgery. *Magn Reson Med* 1994;31:628-36.
19. Hall AS, Prior MV, Hand JW, Young IR, Dickinson RJ. Observation by MR imaging of in vivo temperature changes induced by radio frequency hyperthermia. *J Comput Assist Tomogr* 1990;14:430-6.

20. Matsumoto R, Oshio K, Jolesz FA. Monitoring of laser and freezing-induced ablation in the liver with T1-weighted MR imaging. *J Magn Reson Imaging* 1992;2:555-62.
21. Zhang Z. Dynamic temperature mapping – real-time MRI strategies and model-based reconstructions. University of Göttingen, PhD Thesis 2016.
22. Peters RD, Hinks RS, Henkelman RM. Ex vivo tissue-type independence in proton-resonance frequency shift MR thermometry. *Magn Reson Med* 1998;40:454-9.
23. Teichmann HO, Herrmann TR, Bach T. Technical aspects of lasers in urology. *World J Urol* 2007;25:221-5.
24. Bach T, Herrmann TR, Ganzer R, Burchardt M, Gross AJ. RevoLix vaporessection of the prostate: initial results of 54 patients with a 1-year follow-up. *World J Urol* 2007;25:257-62.
25. Weidensteiner C, Kerioui N, Quesson B, de Senneville BD, Trillaud H, Moonen CT. Stability of real-time MR temperature mapping in healthy and diseased human liver. *J Magn Reson Imaging* 2004;19:438-46.
26. Rieke V, Butts Pauly K. MR thermometry. *J Magn Reson Imaging* 2008;27:376-90.
27. Merboldt KD, Uecker M, Voit D, Frahm J. Spatially encoded phase-contrast MRI-3D MRI movies of 1D and 2D structures at millisecond resolution. *Magn Reson Med* 2011;66:950-6.
28. Tan Z, Roeloffs V, Voit D, Joseph AA, Untenberger M, Merboldt KD, Frahm J. Model-based reconstruction for real-time phase-contrast flow MRI: Improved spatiotemporal accuracy. *Magn Reson Med* 2017;77:1082-93.
29. Mei CS, Panych LP, Yuan J, McDannold NJ, Treat LH, Jing Y, Madore B. Combining two-dimensional spatially selective RF excitation, parallel imaging, and UNFOLD for accelerated MR thermometry imaging. *Magn Reson Med* 2011;66:112-22.

Cite this article as: Zhang Z, Michaelis T, Frahm J. Towards MRI temperature mapping in real time—the proton resonance frequency method with undersampled radial MRI and nonlinear inverse reconstruction. *Quant Imaging Med Surg* 2017;7(2):251-258. doi: 10.21037/qims.2017.03.03